Spatial and Temporal Mapping of Key Lipid Species in *Brassica napus* Seeds[1][CC-BY]

Helen K. Woodfield[2], Drew Sturtevant[2], Ljudmilla Borisjuk, Eberhard Munz, Irina A. Guschina, Kent Chapman*, and John L. Harwood*

Cardiff School of Bioscience, Cardiff University, Cardiff CF10 3AX, United Kingdom (H.K.W., I.A.G., J.L.H.); Department of Biological Sciences, Center for Plant Lipid Research, University of North Texas, Denton, Texas 76203-5017 (D.S., K.C.); and Leibniz Institute of Plant Genetics and Crop Research, D-06466 Gatersleben, Germany (L.B., E.M.)

ORCID IDs: 0000-0002-0839-6105 (H.K.W.); 0000-0001-6910-0841 (L.B.); 0000-0002-4994-3304 (E.M.); 0000-0003-0489-3072 (K.C.); 0000-0003-2377-2612 (J.L.H.).

The regulation of lipid synthesis in oil seeds is still not fully understood. Oilseed rape (*Brassica napus*) is the third most productive vegetable oil crop on the global market; therefore, increasing our understanding of lipid accumulation in oilseed rape seeds is of great economic, as well as intellectual, importance. Matrix-assisted laser/desorption ionization-mass spectrometry imaging (MALDI-MSI) is a technique that allows the mapping of metabolites directly onto intact biological tissues, giving a spatial context to metabolism. We have used MALDI-MSI to study the spatial distribution of two major lipid species, triacylglycerols and phosphatidylcholines. A dramatic, heterogenous landscape of molecular species was revealed, demonstrating significantly different lipid compositions between the various tissue types within the seed. The embryonic axis was found to be particularly enriched in palmitic acid, while the seed coat/aleurone layer accumulated vaccenic, linoleic, and α-linoleic acids. Furthermore, the lipid composition of the inner and outer cotyledons differed from each other, a remarkable discovery given the supposed identical functionality of these two tissues. Triacylglycerol and phosphatidylcholine molecular species distribution was analyzed through a developmental time series covering early seed lipid accumulation to seed maturity. The spatial patterning of lipid molecular species did not vary significantly during seed development. Data gathered using MALDI-MSI was verified through gas chromatography analysis of dissected seeds. The distinct lipid distribution profiles observed imply differential regulation of lipid metabolism between the different tissue types of the seed. Further understanding of this differential regulation will enhance efforts to improve oilseed rape productivity and quality.

Global consumption of oil has increased steadily at an annual rate of about 5% for the past 50 years, with only four crops (oil palm [*Elaeis guineensis*], soybean [*Glycine max*], oilseed rape [*Brassica napus*], and sunflower [*Helianthus annuus*]) accounting for 88% of vegetable oil produced. Oilseed rape contributes about 16% of the total global plant production and is the predominant crop in northern Europe and Canada. As worldwide consumption of oil continues to rise, it is vital that we improve our understanding of lipid accumulation in plants, such as oilseed rape, to increase oil production and enable changes to be made to oil quality.

In Arabidopsis (*Arabidopsis thaliana*), at least 600 genes are involved in acyl-lipid metabolism, regulating over 120 enzymatic reactions (Li-Beisson et al., 2010). Given this complexity, it is hardly surprising that our understanding of the regulation of lipid metabolism is incomplete (Weselake et al., 2009; Chapman and Ohlrogge, 2012; Harwood and Guschina, 2013; Bates, 2016). Oilseed rape is the third most productive oil crop on the global market. It is grown predominantly in Europe and Canada and is commercially important to both industrial and food trades. There are two classes of oilseed rape distinguishable by their oil composition: these are known as low erucic acid (LEAR; also known as canola in Canada) and high erucic acid (HEAR) varieties. Both are economically important, with LEAR varieties having more applications in the food industry while HEAR varieties are used predominantly for industrial purposes. The high erucate content of HEAR varieties (~45%) has been suggested to be toxic to

[1] This work was supported by the Biotechnology and Biological Sciences Research Council.

[2] These authors contributed equally to the article.

* Address correspondence to kent.chapman@unt.edu or harwood@cardiff.ac.uk.

The author responsible for distribution of materials integral to the findings presented in this article in accordance with the policy described in the Instructions for Authors (www.plantphysiol.org) is: John L. Harwood (harwood@cardiff.ac.uk).

J.L.H. conceived the original research plans; K.C. and J.L.H. supervised the experiments; H.K.W. and D.S. carried out most of the experiments, with equal contributions; I.A.G. carried out lipid analysis; E.M. and L.B. provided the magnetic resonance imaging data; H.K.W., D.S., K.C., and J.L.H. analyzed the data; J.L.H. conceived the project; H.K.W. wrote the article with contributions from all the authors.

www.plantphysiol.org/cgi/doi/10.1104/pp.16.01705

humans, which in part led to the development of the LEAR varieties for culinary use. The seeds of LEAR oilseed rape varieties, such as that focused on in this study, typically accumulate about 45% oil by dry weight that is rich in oleic (~62%), linoleic (~22%), and α-linolenic (~10%) acids and are safe for human consumption. Oilseed rape is a close relative of the model plant Arabidopsis, so it is often possible to complement discoveries made in the crop with the huge reserve of genetic resources available from the model plant. This, along with the clear economic importance of the crop, makes oilseed rape an excellent subject for studies such as those presented here.

Lipid accumulation in seeds follows a sigmoidal curve pattern over time and can be split into three distinct phases. Early in seed development, lipid accumulation is relatively slow, then around the midpoint of development, there is a period of rapid lipid accumulation, which plateaus as the seed approaches maturity. The study of lipidomics in developing seeds can give insight into the regulation of metabolic processes involved in storage lipid accumulation. Lipidomic studies typically employ solvent extraction-based methods, which can include a wide range of metabolites with different chemical properties. However, a consequence of using these methods is that the spatial context of where the metabolites originated from is lost. Imaging-based mass spectrometry (MS) approaches have emerged as an alternative, or as an addition to these extraction based methods, to provide an additional spatial dimension to metabolomic studies. Matrix-assisted laser/desorption ionization-mass spectrometry imaging (MALDI-MSI) is a powerful analytical technique that enables the spatial mapping of metabolites within intact biological tissues or directly off tissue surfaces (Cornett et al., 2007; Horn and Chapman, 2014; Sturtevant et al., 2016). This analytical technique was pioneered by the Caprioli group in the 1990s in animal systems (Caprioli et al., 1997) and, over the last decade, has been applied to plant systems to great effect (Horn and Chapman, 2014; Korte et al., 2015; Boughton et al., 2016). Applying MALDI-MSI to the analysis of lipids in oilseeds will better our understanding of lipid metabolism, knowledge that may be important for crop improvement (Haslam et al., 2016). Moreover, observing the spatial context of lipid distribution gives new insights into how associated metabolic networks might be differentially regulated between different tissue types. MALDI-MSI has been used previously with great success to show the spatial heterogeneity of lipid distribution in various plant seeds, such as cotton (*Gossypium hirsutum*; Horn et al., 2012; Sturtevant et al., 2017b), maize (*Zea mays*; Feenstra et al., 2015), camelina (*Camelina sativa*; Horn et al., 2013), and Arabidopsis (Sturtevant et al., 2016, 2017a), all of which show a certain degree of tissue-specific lipid accumulation across several different lipid classes.

Other in situ imaging techniques have been used to visualize lipid distribution within tissues, including ^{1}H-NMR imaging. Borisjuk et al. (2013) showed that, in developing oilseed rape embryos, the initial deposition of lipids began in the aleurone layer and endosperm followed by a substantial increase of accumulation within the embryo throughout seed development. However, these data gave no information about the spatial distribution of individual lipid classes or molecular species, information that is needed to evaluate the details of oil accumulation. An alternative to imaging lipid distribution in situ is lipid analysis of dissected tissues. Indeed, a study using Arabidopsis seeds revealed a tissue-specific variation in the fatty acid composition of total lipids (Li et al., 2006). However, individual lipid classes were not analyzed.

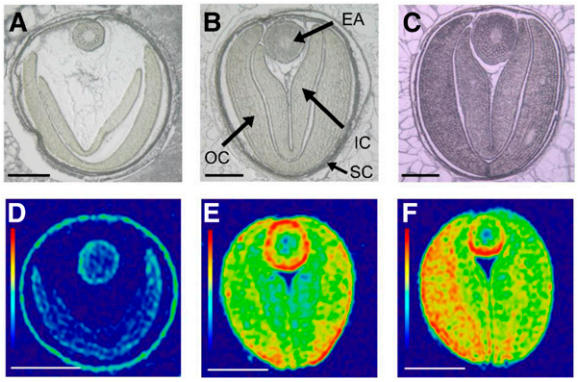

Figure 1. NMR visualization of total lipid distribution within oilseed rape seeds at three developmental stages. A to C, Bright-field images of transverse sections of oilseed rape seeds at 20 d after flowering (DAF; A), 27 DAF (B), and 35 DAF (C). Bars = 1 mm. Labels show embryonic axis (EA), outer cotyledon (OC), inner cotyledon (IC), and seed coat/aleurone layer (SC). D to F, Two-dimensional images represent three-dimensional data sets from intact seeds at 20 DAF (D), 27 DAF (E), and 35 DAF (F). Bars = 1.5 mm. The lipid content is color coded (red = maximal signal and blue = minimal signal) and normalized.

Here, we used MALDI-MSI, ^{1}H-NMR imaging, and dissected embryos to analyze the spatial distribution of two key lipid classes, phosphatidylcholines (PCs) and triacylglycerols (TAGs), throughout the development of oilseed rape seeds. Both lipid classes showed dramatic patterns of tissue-specific accumulation, which contribute to our understanding of oil accumulation in this important crop.

RESULTS

NMR Imaging of Oilseed Rape Seed Oil

An oilseed rape embryo comprises a central embryonic axis (which will develop into the hypocotyl and the root) embraced by two cotyledons. This embryo is encased by a liquid endosperm, a cellular aleurone layer, and a seed coat. As the seed develops and the embryo expands, the two cotyledons fold in toward the embryonic axis, one staying outermost while the other becomes restricted to the inner part of the seed. These two cotyledons are referred to as the outer and inner cotyledons, respectively. These anatomical structures of

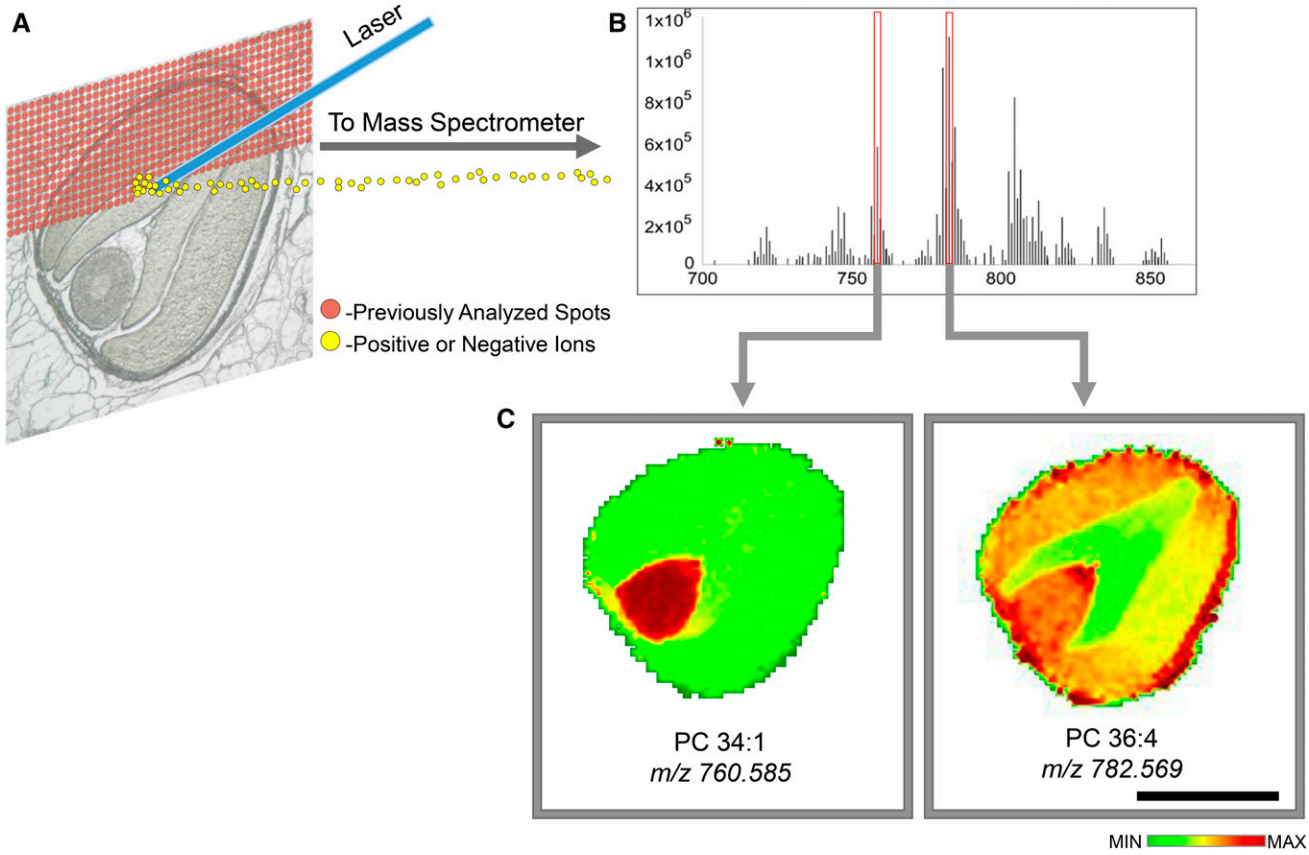

Figure 2. Schematic showing the MALDI-MSI method. A, A laser is rastered over a matrix-coated seed section in a series of spot points with a given *x-y* coordinate. The example shown is an oilseed rape seed representative section (30 μm thickness). B, The ions produced are directed to a mass spectrometer, where their *m/z* values are measured. C, Metabolites are identified, and false-color images are generated to depict the ion intensity at each laser spot point. Bar = 1 mm.

the seed are annotated in representative bright-field images of cryosections from each of the developmental time points examined here (Fig. 1). Noninvasive imaging of intact seeds by ^{1}H-NMR imaging was used to establish the spatial localization of total lipids in developing oilseed rape seeds (Fig. 1; Neuberger et al., 2008, 2009).

Oilseed rape seeds were collected at three key developmental time points, 20, 27, and 35 DAF, corresponding to early, mid, and late stages of lipid accumulation, respectively. At 20 DAF, the lipid signal was highest within the aleurone layer and seed coat, with a small amount in the embryonic tissues. However, no lipid accumulation was seen in the liquid endosperm portion of the seed (Fig. 1). Lipid accumulation increased through seed development, primarily in embryonic tissues. At both the 27- and 35-DAF time points, lipid deposition was particularly prevalent around the outer edges of the embryonic axis and outer cotyledon. These NMR distribution profiles in oilseed rape are supported by data published by Borisjuk et al. (2013). Additionally, ^{1}H-NMR imaging has been used to map spatial differences in lipid distribution in other oil seeds, including cotton (Horn et al., 2012) and camelina (Horn et al., 2013). Considering that these heterogenous and tissue-specific differences in lipid accumulation are observed across different plant families, it implies a conserved mechanism to store lipids during seed development.

Spatial Mapping of PC and TAG at the Midpoint of Seed Lipid Accumulation

In addition to where total lipids accumulated, we examined whether individual lipid molecular species of TAG and PC (as key lipid classes seen during seed development) were located differentially within the seed and if these distributions changed during development. MALDI-MSI was used to investigate the in situ distribution profiles of molecular species of PC and TAG, major membrane and storage lipids, respectively, in medial, transverse cryosections of developing oilseed rape seeds at 20, 27, and 35 DAF. MALDI-MSI is achieved by rastering a laser over the entire surface of a tissue (here every 40 μm for oilseed rape seeds), collecting a mass spectrum at each x and y coordinate. These mass spectra can then be searched for the mass-to-charge ratio (m/z) of ions of interest, and a heat map

or matrix-assisted laser/desorption ionization-mass spectrometry (MALDI-MS) image is generated representing the spatial localization of the ions in question. A summary of the MALDI-MS imaging for the in situ visualization of TAG and PC is shown in Figure 2, but for more detailed descriptions, see Horn and Chapman (2014) and Sturtevant et al. (2016).

MALDI-MS images of oilseed rape seed sections for PC and TAG at the midpoint in oil accumulation, 27 DAF, are presented using two different intensity scales (Figs. 3 and 4). All PC and TAG MALDI-MS images in Figures 3 and 4, respectively, are set to the same intensity scale. Scaling the images in this manner allows for direct comparisons of the relative abundances across all images for individual PC or TAG molecular species. These scaled MALDI-MS images revealed that the most abundant PC molecular species at 27 DAF was PC-36:2 (18:1/18:1; Fig. 3A). Similarly, TAG molecular species TAG-54:3 (18:1/18:1/18:1) and, to a lesser extent, TAG-52:4 (18:1/18:1/16:0) and TAG-54:4 (18:1/18:1/18:2) were the most abundant TAG species observed within the seed at this stage of development (Fig. 4A). These results were expected, given that 18:1 is the most abundant fatty acid in LEAR (canola) varieties of oilseed rape (Gunstone et al., 2007). Scaling MALDI-MS images to a fixed value had a disadvantage in that the spatial distribution of lipid molecular species can be difficult to discern for species that comprise lowest or highest amounts in the tissues (they tend to be washed out, in green, in false color images or maxed out, in dark red). To overcome this, the scale can be adjusted for maximum ion intensity (converted to mol %) in each MALDI-MS image to reveal and emphasize the distribution of particular lipid molecular species within the seed.

Adjustment of the scale of each image to emphasize distribution patterns revealed a dramatic tissue-specific distribution of PC molecular species (Fig. 3B). For instance, the embryonic axis had highest relative levels of PC species containing 16:0 (e.g. PC-34:1 [18:1/16:0]). In contrast, the seed coat/aleurone layer showed highest relative levels of species containing 18:2 and 18:3, such as PC-34:2 (18:2/16:0), PC-34:3 (18:3/16:0), and PC-36:5 (18:3/18:2; Fig. 3B). Most striking of all was a differential enrichment of several PC molecular species between the inner and outer cotyledons, despite the fact that the two tissues are functionally identical. PC-36:1 (18:1/18:0) and PC-36:3 (18:1/18:1) exhibited this difference most dramatically (Fig. 3B). The distributions of PC-36:1 and PC-36:3 were markedly different from that of PC-36:2, the major PC molecular species. We confirmed that the distribution of isotopomers of PC-36:2 did not distort the observed distributions of PC-36:1 because, for example, the M+2 isotopomer of PC-36:2 is easily distinguished by the high-resolution MS at 60,000 resolving power (Supplemental Fig. S1). Across the PC molecular species examined here, the outer cotyledon was enriched in species containing 18:2 and 18:3 fatty acids compared with the inner cotyledon, while the inner cotyledon accumulated predominantly PC molecular species containing 18:0 and 18:1 fatty acids.

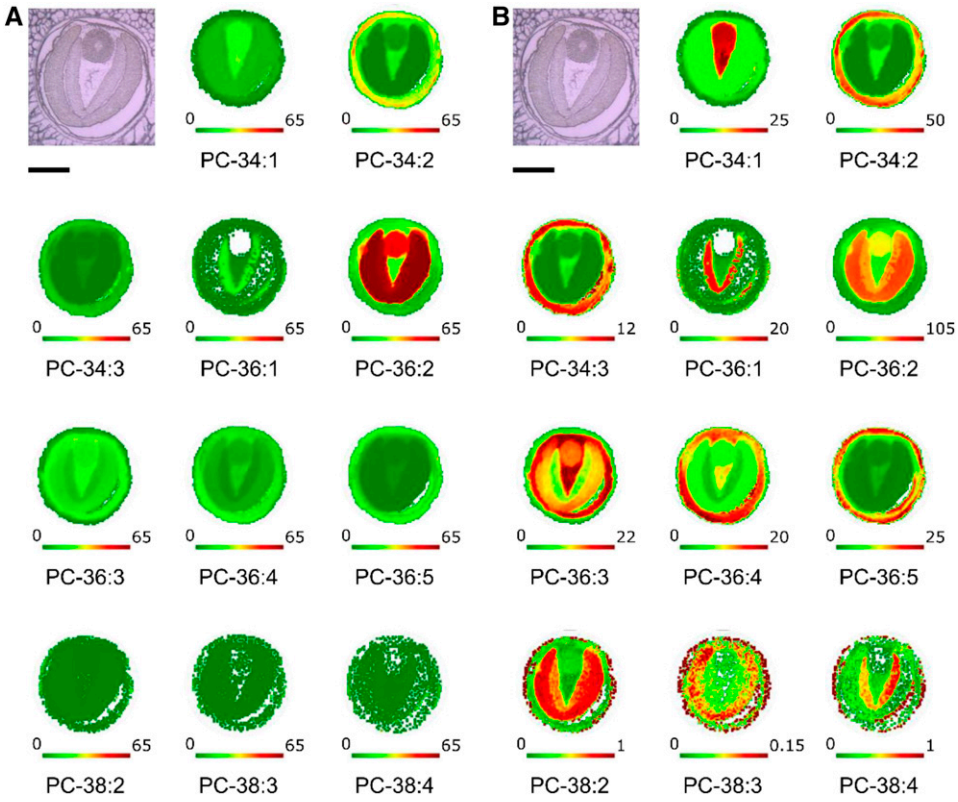

Figure 3. Imaging of selected PC molecular species in oilseed rape seeds at 27 DAF. Bright-field images of seed cross sections at 27 DAF are shown at top left of each part. Bars = 1 mm. The distributions of selected PC molecular species are shown with a fixed mol % to show absolute distribution profiles (A) and an adjusted mol % to show relative distribution profiles (B). Below each image is a color scale bar, with green and red representing low and high levels, respectively. Numbers at either end of the colored bar represent the scale of that image. Each image also is labeled with the total number of acyl carbons and double bonds (e.g. PC-34:1).

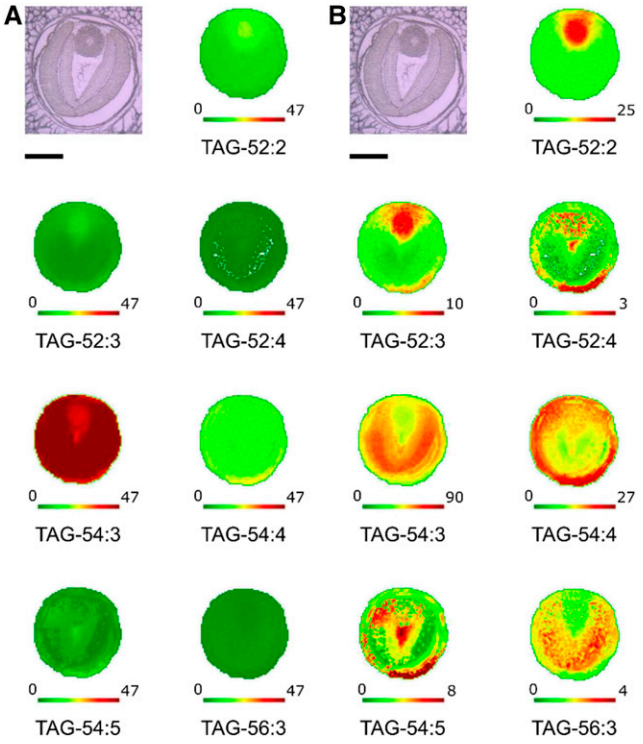

Figure 4. Imaging of selected TAG molecular species in oilseed rape seeds at 27 DAF. Bright-field images of seed cross sections at 27 DAF are shown at top left of each part. Bars = 1 mm. The distributions of selected TAG molecular species are shown with fixed mol % to show absolute distribution profiles (A) and adjusted mol % to show relative distribution profiles (B). Below each image is a color scale bar, with green and red representing low and high levels, respectively. Numbers at either end of the colored bar represent the scale of that image. Each image also is labeled with the total number of acyl carbons and double bonds (e.g. TAG-52:2).

TAG molecular species also showed tissue-specific differences in TAG composition (Fig. 4B) when scaled to emphasize distribution patterns. As with PC, TAG molecular species also showed differential enrichment between the cotyledons and embryonic axis. TAG-54:3 (18:1/18:1/18:1) was localized predominantly to the cotyledons, which was expected given that TAG-54:3 is the most abundant TAG species present in the seed and that the cotyledons make up the bulk of the volume of the embryo (Fig. 4B). As with PC, the embryonic axis had highest relative levels of molecular species containing 16:0, such as TAG-52:2 and TAG-52:3. However, unlike the PC distribution profiles, the inner and outer cotyledons did not appear to show dramatic differences in TAG molecular species localization relative to each other. Less distinct distribution patterns were observed for TAG-52:4, TAG-54:4, and TAG-54:5. There was a slight enrichment of signal from these molecular species in the seed coat/aleurone; however, overall, there was little TAG signal from the seed coat/aleurone, reflecting the nonstorage role of these tissue types, especially at later stages of seed development.

Spatial Distribution of PC and TAG Molecular Species through Seed Development

The distribution of PC and TAG molecular species did not change significantly during development (Figs. 5 and 6). Some molecular species, such as PC-34:1 (18:1/16:0) in the embryonic axis and PC-36:3 (18:2/18:1) in the outer cotyledon, retained their tissue specificity from 20 to 35 DAF. Similar trends were observed for TAG molecular species; embryonic axis-localized TAG-52:2 (18:1/18:1/16:0) and cotyledon-localized TAG-54:3 (18:1/18:1/18:1) and TAG-56:3 (18:1/18:1/20:1) maintained their molecular heterogeneity from 20 to 35 DAF. However, there were a few examples where localization did change with development. The most striking was PC-34:2, which was most prevalent in the seed coat/aleurone layer at 20 and 27 DAF but by 35 DAF was concentrated in the embryonic axis region of the embryo (Fig. 5).

In addition to the distribution of most molecular species remaining consistent over time, the relative amount of each lipid species also did not change drastically (Figs. 5 and 6). Three methods of quantifying total amounts of each lipid species were used: ESI-MS, MALDI-MS imaging of tissue, and MALDI-MS analysis of TLE. Relative quantification from these three methods agreed well with each other, and trends were consistent across all three analysis platforms, with only minor differences between the three different analysis methods, two of which were normalized with internal standards (ESI-MS and MALDI-MS of TLE).

TAG molecular species maintained a consistent distribution pattern through seed development, as seen with PC molecular species (Fig. 6). However, while some PC molecular species showed slight variation in distribution through development, there was little to no variation in the distribution of major TAG species. This makes sense, as TAG is a metabolic dead end in the lipid synthesis network, so TAG molecular species will not circulate to other metabolites once accumulated. As with PC, relative amounts of TAG species also remain fairly consistent throughout development (Fig. 6).

Lipid Composition of Dissected Seed Tissues

There are some limitations associated with the MALDI-MSI technique, including ion suppression, absolute quantitation, and the fact that any single tissue section may not represent the entire embryo in three dimensions, so a second approach was used to assess the validity of the MALDI-MSI data acquired. Oilseed rape seeds from three developmental time points (20, 27, and 35 DAF) were dissected by hand into four component tissue types: seed coat (plus aleurone layer), embryonic axis, inner cotyledon, and outer cotyledon. Lipids from these tissues were separated into lipid classes by thin-layer chromatography (TLC), and the fatty acid composition of each lipid class was determined by gas chromatography (GC). The fatty acid composition of both PC and TAG

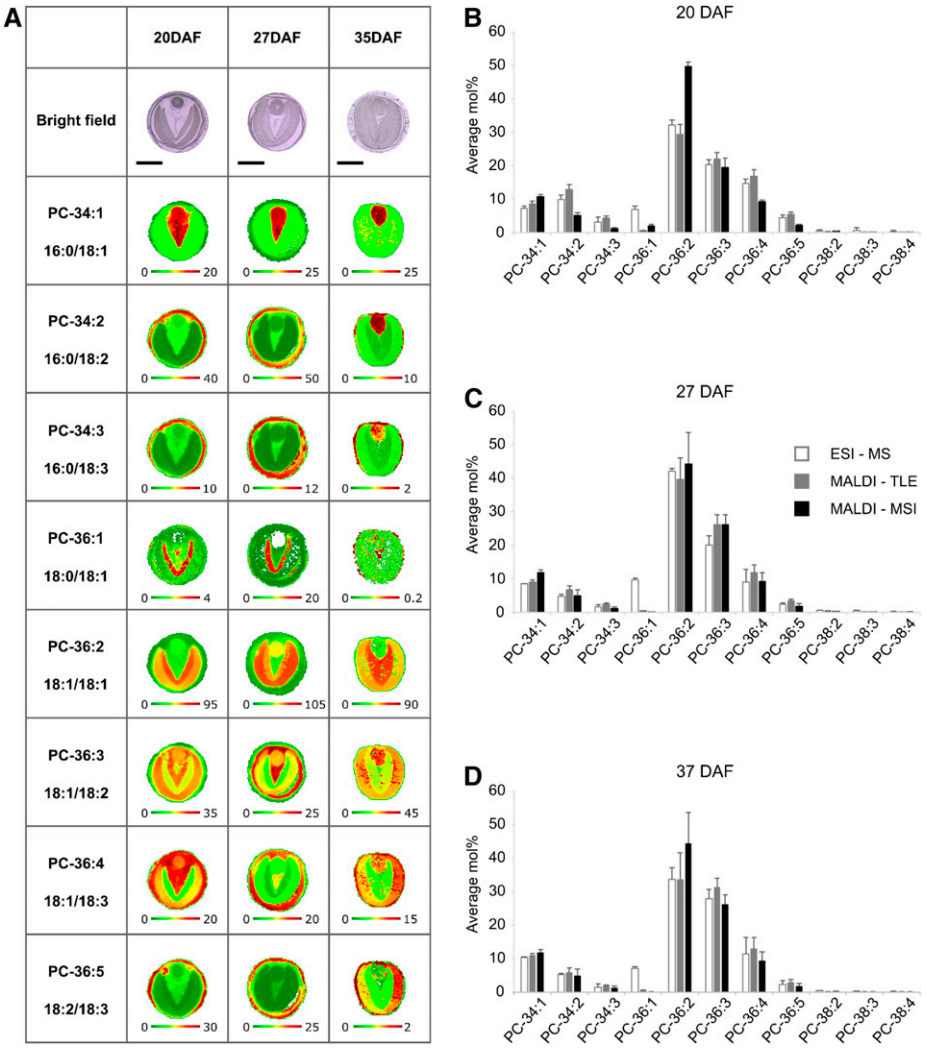

Figure 5. Imaging and quantification of selected PC molecular species in oilseed rape seeds at three developmental stages. A, Bright-field images of seed cross sections (top of each column; bars = 1 mm) and relative distribution patterns of selected PC species at three time points, 20, 27, and 35 DAF (one developmental stage per column) are shown. Below each image is a color scale bar, with green and red representing low and high levels, respectively. Numbers at either end of the colored bar represent the scale of that image. PC species with total number of acyl carbons and number of double bonds, along with the most likely acyl combination (based on MS data) below, are indicated at left. B and C, Quantification of total molecular species by electrospray ionization-mass spectrometry (ESI-MS; white; $n = 3$), MALDI-MS of total lipid extracts (TLE; gray; $n = 3$), and MALDI-MSI (black; $n = 3$) is compared at three developmental stages. Quantification in lipid extracts was based on internal standards. Values shown are means ± SD.

molecular species supports the data obtained through MALDI-MSI analysis (Figs. 7 and 8). For instance, MALDI-MS images showed an enrichment of molecular species containing 16:0 in the embryonic axis, such as PC-34:1 and TAG-52:2, which was corroborated by GC data. At all three time points, TAG had significantly higher 16:0 in the dissected embryonic axis compared with other tissue types and PC had higher levels of 16:0 relative to the cotyledons, but, unlike TAG, the seed coat had similar levels of 16:0 to the embryonic axis. MALDI-MSI also showed enrichment of PC species containing 18:2 and 18:3 in the seed coat/aleurone layer, which is reflected in the fatty acid composition of PC obtained through GC analysis (Fig. 7; for a schematic representation of these data, see Supplemental Fig. S2).

In addition to corroborating the MALDI-MSI data, GC analysis of dissected tissues revealed a further surprising result. For all lipid classes examined, the seed coat/aleurone layer had a dramatically different fatty acid profile compared with the embryonic tissues. The seed coat/aleurone layer had high levels of 18:1 n7 and low 18:1 n9 compared with other tissue types. In addition, the seed coat/aleurone layer contained much higher levels of polyunsaturated fatty acids compared with the embryonic tissues. This was the case for all lipid species examined, including PC, TAG, diacylglycerol, monogalactosyldiacylglycerol, digalactosyldiacylglycerol, phosphatidic acid, phosphatidylethanolamine, phosphatidylglycerol, and phosphatidylinositol (Figs. 7 and 8; Supplemental Tables 1–9).

DISCUSSION

Heterogenous Spatial Distribution of PC and TAG in Oilseed Rape Seeds

MS-based imaging of oilseed rape seeds showed striking heterogenous distribution patterns of PC and TAG, which would not have been revealed when studying these seeds using regular extraction-based analytical techniques. The spatial heterogeneity of

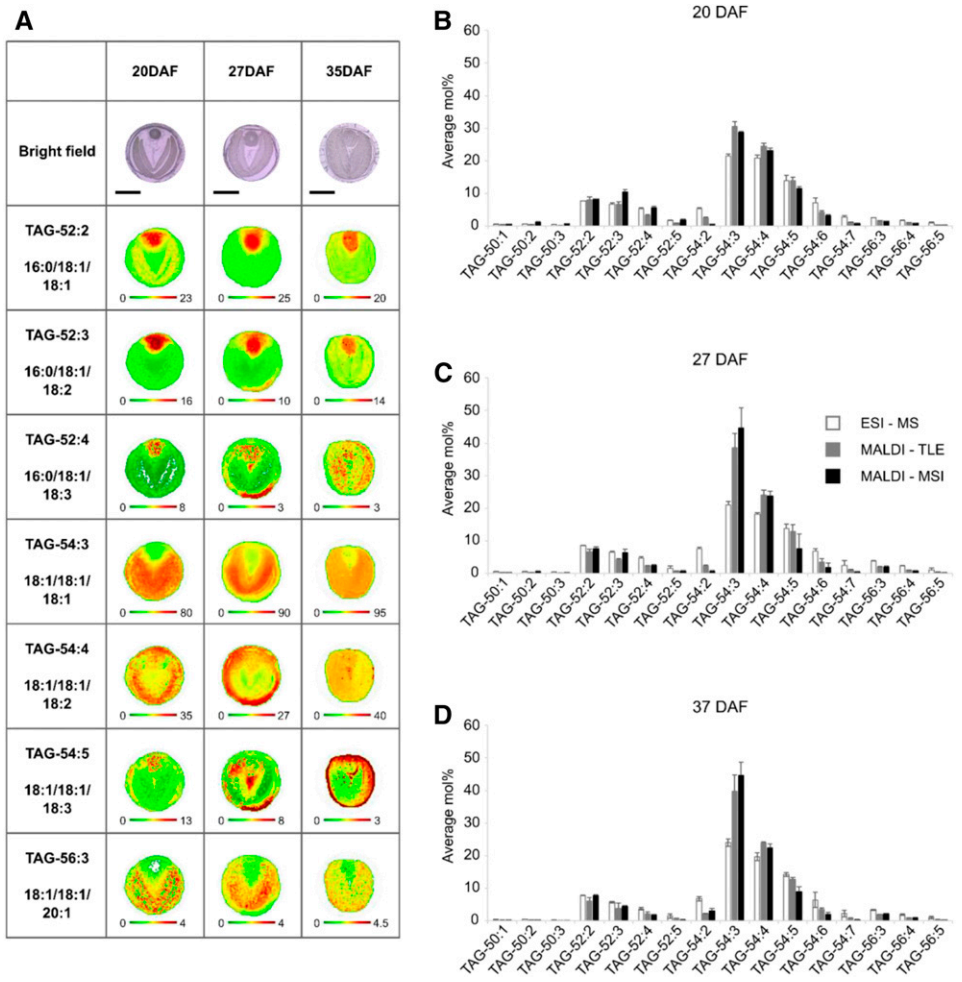

Figure 6. Imaging and quantification of selected TAG molecular species in oilseed rape seeds at three developmental stages. A, Bright-field images of seed cross sections (top of each column; bars = 1 mm) and relative distribution patterns of selected TAG species at three time points, 20, 27, and 35 DAF (one developmental stage per column) are shown. Below each image is a color scale bar, with green and red representing low and high levels, respectively. Numbers at either end of the colored bar represent the scale of that image. TAG species with total number of acyl carbons and number of double bonds, along with the most likely acyl combination (based on MS data) below, are indicated at left. B and C, Quantification of total molecular species by ESI-MS (white; $n = 3$ independent extractions), MALDI-MS of TLE (gray; $n = 3$ independent extractions), and MALDI-MSI (black; $n = 3$ sections from three different seeds) is compared at three developmental stages. Quantification in lipid extracts was based on internal standards. Values shown are means ± SD.

lipid distribution observed here gives a tantalizing insight into the possibilities of cell-specific regulation of lipid metabolism throughout embryogenesis.

Differences in the patterning of lipid species suggest the tissue-specific expression of enzymes involved in lipid biosynthesis. For instance, both MALDI-MS images and analysis of fatty acid composition showed that the seed coat/aleurone layer had higher levels of lipid species containing 18:2 and 18:3 compared with embryonic tissue types. This may be due to significant levels of the endoplasmic reticulum-localized fatty acid desaturases FAD2 and FAD3 in the seed coat/aleurone layer, which catalyze the conversion of 18:1 to 18:2 and then to 18:3, respectively (Wallis and Browse, 2002). However, there is evidence to suggest that the increased desaturation seen in the peripheral endosperm/aleurone layer in the related plant species, Arabidopsis, is due to the prokaryotic pathway desaturase FAD6 (D. Sturtevant and K. Chapman, unpublished data). Moreover, gene expression mapping of Arabidopsis seeds also suggests that FAD6, FAD7, and FAD8 are all expressed in the peripheral endosperm/aleurone cellular layer, adding further evidence that the unsaturated PC species enriched there are acted on by these enzymes (Ohlrogge and Jaworski, 1997; Schmid et al., 2005). Given that nearly all lipid classes (synthesized in the plastid or endoplasmic reticulum) showed higher levels of desaturation in the seed coat/aleurone layer compared with embryonic tissues (Supplemental Tables 1–9), it is possible that both endoplasmic reticulum- and plastid-localized desaturases are correspondingly more highly expressed in the seed coat and aleurone layer of oilseed rape.

There is a precedent for the embryo-specific expression of genes involved in lipid biosynthesis. For example, in Arabidopsis, *FATTY ACID ELONGATION1* (*AtFAE1*), which is the key enzyme responsible for the elongation of oleoyl-CoA to gondoyl-CoA in the acyl-CoA pool, is expressed exclusively in the cotyledons (Rossak et al., 2001). Here, the MALDI-MS image of TAG-56:3 (18:1/18:1/20:1), a 20:1-containing TAG, was enriched in the cotyledons relative to the embryonic axis (Fig. 6), which corroborates that the enzyme responsible, *FAE1*, and the downstream metabolite are localized in the same tissue.

A common trend seen within embryonic tissues was an enrichment of palmitate containing PC and TAG molecular species (e.g. PC-34:1, TAG-52:2, and TAG-52:3; Figs. 5 and 6) in the embryonic axis compared

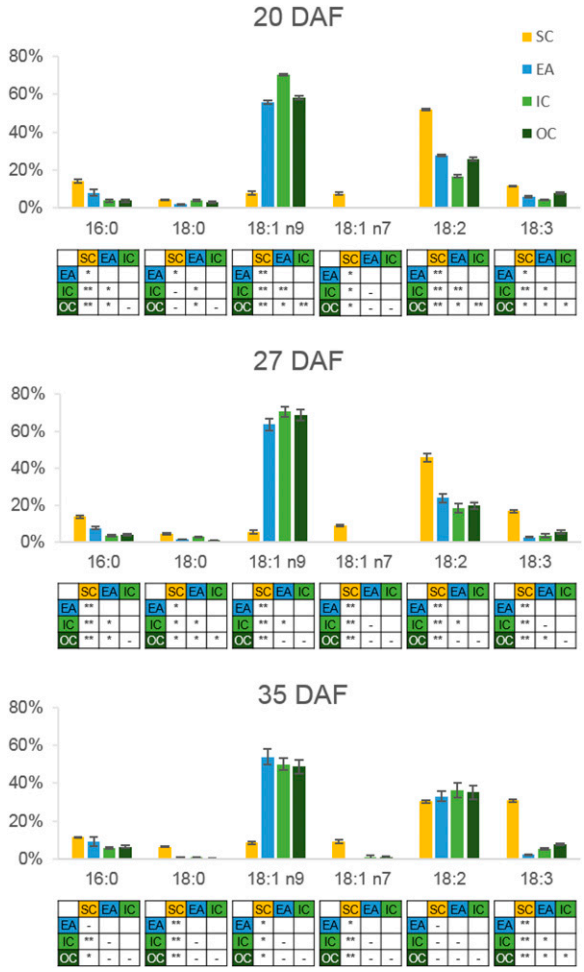

Figure 7. Fatty acid composition of PC in dissected seed tissues at three developmental stages. Tissues analyzed were the seed coat/aleurone layer (SC), embryonic axis (EA), inner cotyledon (IC), and outer cotyledon (OC). Seeds were sampled at 20, 27, and 35 DAF. Values are means ± SD (n = 3). Tables below each graph show the statistical analysis of the fatty acid in the column immediately above: *, $P < 0.05$; **, $P < 0.001$; –, no significant difference.

with the cotyledons. This distribution relationship has been seen in other oil seeds, such as cotton and camelina (Horn et al., 2012, 2013). A potential explanation for this distribution in acyl composition could be a spatial difference in the expression of the thioesterases FATA and FATB (Wallis and Browse, 2002).

One of the more notable findings of this study was that the inner and outer cotyledons were enriched with different TAG and, especially, PC molecular species, despite being functionally similar tissues. It was shown previously that the inner and outer cotyledons accumulate total lipids at different rates, but these differences even out as the seed reaches full maturity (Borisjuk et al., 2013). We have shown through MALDI-MSI and fatty acid profiling of dissected seeds that these differences extend to individual molecular species within numerous lipid classes, especially in PC. In addition, our MALDI-MS images show these differential accumulation patterns generally persisting throughout the period of oil accumulation. One explanation for the difference seen between inner and outer cotyledons is that the outer cotyledon would receive more light and oxygen than the inner cotyledon, which could have a marked effect on the levels of photosynthesis and the reducing power of the cells in each tissue. An alternative theory is that, during embryo folding, the inner cotyledon is put under higher physical constraints than the outer cotyledon, which alters the metabolism within this tissue compared with the outer cotyledon (Borisjuk et al., 2013). Interestingly, imaging of TAG accumulation did not reveal as many significant differences between the inner and outer cotyledons. However, this may have been due to the presence of isobaric species that are harder to distinguish in TAG, with three fatty acid chains, compared with PC, which only has two. For example, the signal for TAG-54:4 is fairly uniform between the inner and outer cotyledons, but one cotyledon may be accumulating 18:1/18:1/18:2 while the other could be enriched with 18:0/18:1/18:3. TAG production involves significant flux through PC in a process known as acyl editing (Bates and Browse, 2011; Bates et al., 2012), which would logically lead to the suggestion that, if there is a difference between the two tissue types in PC molecular species, there is likely to be a similar difference in TAG molecular species. Indeed, comparison of the fatty acid composition of dissected seed tissues shows a similar degree of significant differences between inner and outer cotyledons in both PC and TAG species.

Comparison of Lipid Distribution in Oilseed Rape Compared with Other Oilseed Species

The recently developed oilseed crop camelina also has been analyzed for the spatial distribution of lipid molecular species within the seed (Horn et al., 2013). Some lipid molecular species in camelina have similar distribution patterns to oilseed rape, such as PC-34:2, which accumulated in the embryonic axis, whereas other molecular species do not match, such as PC-36:2, which is enriched in the cotyledons of oilseed rape but has a uniform distribution in camelina. Camelina has higher levels of total polyunsaturated fatty acids compared with oilseed rape, which may explain why not all molecular species have comparable spatial distributions. Moreover, in high-oleate mutant camelina lines, which have a similar fatty acid profile to oilseed rape, many of the differences in lipid accumulation patterns seen between oilseed rape and wild-type camelina are lost. For instance, PC-36:2, which had a uniform distribution in wild-type camelina, was enriched in the cotyledons in the high-oleate mutant (Horn et al., 2013), matching the distribution pattern seen in oilseed rape.

As more MALDI-MSI studies are performed using other oilseed plant species and transgenic oilseed lines, it may be possible to define common principles for lipid accumulation patterns within seeds, according to total

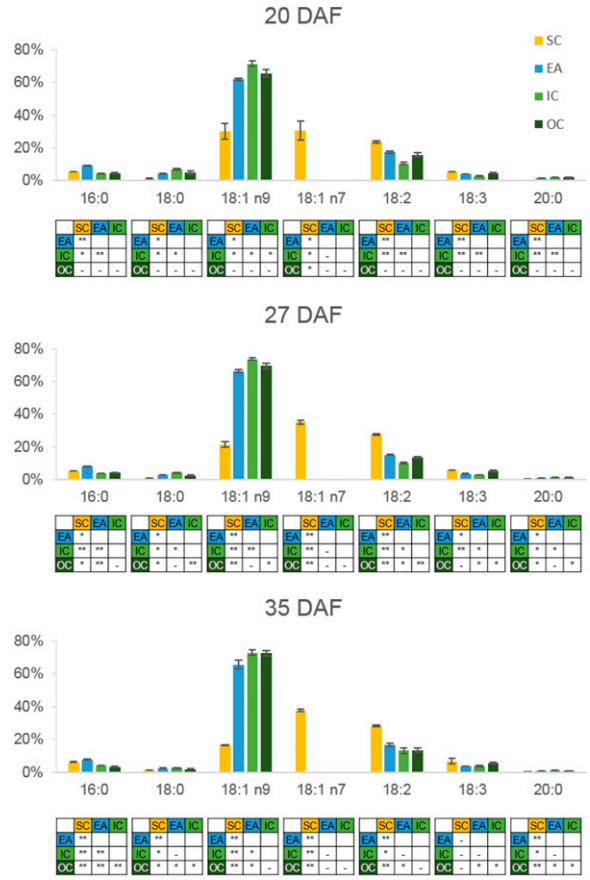

Figure 8. Fatty acid composition of TAG in dissected seed tissues at three developmental stages. Tissues analyzed were the seed coat/aleurone layer (SC), embryonic axis (EA), inner cotyledon (IC), and outer cotyledon (OC). Seeds were sampled at 20, 27, and 35 DAF. Values are means ± SD (n = 3). Tables below each graph show the statistical analysis of the fatty acid in the column immediately above: *, $P < 0.05$; **, $P < 0.001$; –, no significant difference.

fatty acid composition and seed structure. These studies could be complemented by tissue-specific RNA sequencing studies, which would give spatial context to the transcripts of the enzymes that synthesize these lipids. By comparing MALDI-MSI data from a range of different species, it may be possible to infer evolutionarily conserved mechanisms for the tissue-specific regulation of lipid synthesis.

The Seed Coat/Aleurone Layer Has a Distinct Lipid Composition

Of all the tissue types analyzed, the seed coat/aleurone layer stood out as being the most distinct in terms of fatty acid composition. The seed coat is entirely maternal in origin and has been implicated in the control of seed oil synthesis (Radchuk and Borisjuk, 2014). For instance, there is evidence to suggest that the sugar concentration in the seed coat might regulate the efficiency of oil accumulation in the embryo (Liu et al., 2014). We noted that the seed coat/aleurone layer contained a high proportion of 18:1 n7 (vaccenic acid) compared with 18:1 n9 (oleic acid). Accumulation of vaccenic acid also has been reported in Arabidopsis and in HEAR and LEAR varieties of oilseed rape (Penfield et al., 2004; Li et al., 2006; Bryant et al., 2016). ω-7 fatty acids are economically valuable for both industrial and nutraceutical applications (Wu et al., 2012). Their benefits range from improved biodiesel and polymer precursor production (Durrett et al., 2008) to beneficial health properties such as enhanced cardiovascular fitness and reducing LDL cholesterol levels (Curb et al., 2000). However, despite their economic value, there are currently no commercially significant oil crops producing high levels of ω-7 fatty acid-rich oils (Nguyen et al., 2015). Indeed, the physiological role for ω-7 fatty acids in plants is not well understood, and until recently, the biosynthetic pathway used for their production was unclear. Bryant et al. (2016) demonstrated that ACYL-ACYL CARRIER PROTEIN DESATURASE2 (AAD2) and AAD3 are the major Δ9 desaturases responsible for vaccenic acid synthesis in Arabidopsis. The feasibility of engineering plants with high levels of ω-7 fatty acids has been demonstrated in Arabidopsis (Cahoon and Shanklin, 2000; Nguyen et al., 2010) and camelina (Nguyen et al., 2015). However, the most efficient way to engineer high vaccenic acid levels into a high-yielding crop like oilseed rape may be to redirect the endogenous biosynthetic pathway from the seed coat/aleurone layer into the embryonic tissue. This could be achieved by engineering increased expression of AAD2 and AAD3 in the embryo or manipulating the MYB118 regulatory network (Barthole et al., 2014).

CONCLUSION

In summary, visualization of key lipids has highlighted the dramatic metabolic heterogeneity between the different tissues making up the seeds of oilseed rape. Fatty acid analysis of hand-dissected seeds supported the molecular species distribution patterns seen in MALDI-MS images, validating the use of MALDI-MSI as a reliable technique for analyzing lipid distribution and composition in oilseed rape. Concerted efforts are being made to construct a more holistic picture of the regulation of acyl-lipid metabolism (Wang et al., 2015), and here, we add a spatial perspective of lipid metabolism that revealed unexpected complexities to oil accumulation. By combining spatial data from metabolite imaging with these models and spatial mapping of enzyme activity, it will be possible to elucidate the tissue-specific metabolic pathways involved in lipid biosynthesis. This would be of direct importance to efforts in genetic manipulation as well as boosting oil yields. As our understanding of lipid metabolism improves, so too do our chances of developing crops that will meet the challenge of coping with the world's ever-increasing oil consumption.

MATERIALS AND METHODS

Plant Material

Oilseed rape (*Brassica napus* 'Westar') seeds, a kind gift from Dr. R.J. Weselake (University of Alberta, Edmonton), were germinated in damp multipurpose compost (M3 Levington compost) mixed with fine sand (3:1). Seedlings were transplanted to seed trays and grown for 10 d followed by a further transplanting to 8-inch pots. Plants were grown in a greenhouse, temperature regulated to 23°C, with supplemental lighting to maintain a light intensity of 250 μmol m^{-2} s^{-1}. Flowers were hand pollinated and tagged on the day of flower emergence.

Sample Preparation for MALDI-MSI

Siliques were harvested at 20, 27, and 35 DAF. Seeds were dissected from the pods and incubated in 4% paraformaldehyde at room temperature for 30 min to fix the tissue. This fixation treatment was followed by three 5-min washes in 50 mM PIPES-NaOH, pH 7.2. Fixed seeds were then embedded in 10% gelatin and frozen at −80°C for at least 24 h. Samples equilibrated to −20°C were sectioned using an OTF5000 cryostat (Bright) with a constant chamber and chuck temperature of −17°C. Tissue sections of 30 μm were adhered to glass slides (Fisherbrand Superfrost Plus) and freeze dried (Heto PowerDry PL3000; Thermo Scientific) overnight. Sections were stored at room temperature in desiccators to minimize moisture exposure.

MALDI-MSI of Tissue Sections and Extract Analysis

Before MALDI-MSI analysis, paraformaldehyde-fixed and lyophilized oilseed rape seed sections were coated with 2,5-dihydroxybenzoic acid (DHB) by sublimation using a procedure adapted from Hankin et al. (2007). Matrix sublimation of tissues with DHB occurred under vacuum pressure of 100 mTorr at 120°C between 3 and 4 min. Matrix-coated tissues were removed from the sublimation apparatus and immediately used for MALDI-MSI.

MALDI-MSI data were collected using a MALDI-LTQ-Orbitrap XL mass spectrometer (Thermo Scientific). Conditions for imaging were as follows: laser energy was set to 12 μJ per pulse, raster step size was set to 40 μm, step size was one microscan per microstep, and attenuated gain control was set to on. MS imaging data were acquired in positive mode using the Orbitrap mass analyzer with a resolution of 60,000 and *m/z* scan range of 500 to 1200.

Total lipid extracts from developing embryos at all developmental time points were analyzed by MALDI-MS using the same instrument conditions used for MALDI-MSI. Total lipid extracts were diluted 10 times and spotted onto a MALDI-MS 96-well plate (Thermo Scientific). Then, 2 μL of 10 mg mL^{-1} DHB (70:30 acetonitrile:water) was spotted directly on top of the extract spot and dried with N_2 gas.

Raw MALDI-MS data from MS images and total lipid extracts were processed as described by Horn et al. (2012). PC molecular species were detected as $[M+H]^+$ and $[M+K]^+$ ions, and TAG molecular species were detected as $[M+K]^+$ and $[M+Na]^+$ ions (±10 ppm). MALDI-MS images were generated using MetaboliteImager (Horn and Chapman, 2013) by summing the absolute intensity of both adducts of PC and TAG. We examined the distributions of lipid metabolites at 4 ppm tolerance in addition to 10 ppm tolerance, where there was no potential for the overlap of isotopomers, and distributions of lipid metabolites were not substantially different between these two tolerances; however, the signal-to-noise ratio was improved at 10 ppm and the resolution of images was improved, especially for minor species (Supplemental Fig. S1). Consequently, all images are presented at 10 ppm.

Extract Analysis by ESI-MS

Total lipid extracts were analyzed by direct-infusion ESI-MS on an API 3000 Triple Quadrupole Mass Spectrometer (Applied Biosystems/Sciex). For profiling PC and TAG lipid classes, extracts were prepared in two different solvent solutions, 2:1 methanol:$CHCl_3$ (v/v) and 2:1 $CHCl_3$:methanol (v/v), plus 15 mM ammonium acetate. For the quantification of individual PC and TAG species, a standard mix of 30 μg of di14:0-PC (Avanti Polar Lipids) and 300 μg of tri15:0-TAG (Nu-Chek Prep) was added to each total lipid extract prior to analysis. Extracts were analyzed in a method adapted from Devaiah et al. (2006) in which extracts were injected at a flow rate of 20 μL^{-1} min at a spray voltage of +5.5 kV. PC composition was determined from precursor ion scans detecting for *m/z* +184.07. TAG composition was determined from full scans of extracts, and the designation of acyl chains, but not *sn* positions, was determined from neutral loss scans of individual fatty acids (Lee et al., 2011). ESI-MS raw data were processed using the open-source lipid-analysis software LipidomeDB (Zhou et al., 2011).

Fatty Acid Analysis of Lipids from Dissected Seed Tissues

Seed pods were harvested at 20, 27, and 35 DAF, and the seed coat (plus aleurone layer), embryonic axis, and outer and inner cotyledons were dissected by hand using a razor blade. Dissected tissues were incubated with 1.2 mL of isopropanol at 70°C for 30 min followed by a two-phase lipid extraction method (Smith et al., 1982). Nonpolar lipid classes were separated by TLC using a solvent mix of hexane:diethylether:acetic acid (80:20:1, v/v), while polar lipid classes were separated by two-dimensional TLC using, first, chloroform:methanol:water (65:25:4, v/v) followed by chloroform:acetone: methanol:acetic acid:water (50:20:10:10:5, v/v). Lipids were routinely revealed with UV light after spraying with 0.2% (w/v) 8-anilino-1-naphthalenesulfonic acid in anhydrous methanol (Benning et al., 1995). Spots corresponding to lipid classes were scraped from TLC plates, and for each class, fatty acid methyl esters (FAMEs) were prepared by incubation with 3 mL of 2.5% H_2SO_4 in methanol: toluene (2:1, v/v) at 70°C for 2 h. Nervonic acid (24:1) was used as an internal standard. Samples were then mixed with 2 mL of 5% NaCl and 3 mL of hexane, and the upper, hexane phase was collected. Another 3 mL of hexane was added, thorough mixing was carried out, and the hexane layer was collected. The accumulated hexane phases were dried down under nitrogen. FAMEs were separated using a Clarus 500 gas chromatograph with a flame ionization detector (Perkin-Elmer 8500). It was equipped with a 30-m × 0.25-mm i.d. capillary column (Elite 225; Perkin-Elmer). The oven temperature program was set to 170°C for 3 min, increased by 4°C min^{-1} to 220°C, with a final hold for 15 min at 220°C. FAMEs were identified routinely by the comparison of retention time peaks with a GC-411 standard (Nu-Chek Prep) but had been specifically analyzed by GC-MS (Fuschino et al., 2011). Perkin-Elmer TotalChrom software was used for data acquisition.

NMR Imaging

All magnetic resonance imaging data sets were acquired on an 11.7-tesla Bruker wide-bore system (Bruker BioSpin) equipped with an actively shielded Micro 2.5 gradient system (40 mm i.d. and maximum strength of 660 mTorr m^{-1}). A custom-built 5-mm i.d. Helmholtz coil was used for measurement of the intact seeds. Seeds at different developmental stages were dissected from the silique and placed into a 5-mm NMR tube filled with deuterium oxide. A standard multislice multiecho spin-echo sequence with adjusted chemical shift-selective pulses was applied to acquire high-resolution lipid images of the seed. An isotropic resolution of up to 50 μm in the seeds could be achieved (experimental time of 11 h). One echo with an echo time of 8.2 ms was acquired in the multislice multiecho spin-echo sequence. The repetition time was set to 1,000 ms. Due to the uniform B1 field of the Helmholtz coil used, a correction for B1 inhomogeneity was not necessary. The reconstruction of the acquired data set was conducted using MATLAB (The Mathworks). To generate the visualization of the seeds, the three-dimensional data set was imported into AMIRA (Mercury).

Supplemental Data

The following supplemental materials are available.

Supplemental Figure S1. Threshold differences of MALDI-MS images.

Supplemental Figure S2. Schematic representation of fatty acid distribution in dissected seed tissue at the midpoint of lipid accumulation.

Supplemental Table S1. Fatty acid composition of TAG of dissected oilseed rape seeds

Supplemental Table S2. Fatty acid composition of diacylglycerol of dissected oilseed rape seeds

Supplemental Table S3. Fatty acid composition of phosphatidic acid of dissected oilseed rape seeds

Supplemental Table S4. Fatty acid composition of monogalactosyldiacylglycerol of dissected oilseed rape seeds

Supplemental Table S5. Fatty acid composition of digalactosyldiacylglycerol of dissected oilseed rape seeds

Supplemental Table S6. Fatty acid composition of phosphatidylethanolamine of dissected oilseed rape seeds

Supplemental Table S7. Fatty acid composition of phosphatidylglycerol of dissected oilseed rape seeds

Supplemental Table S8. Fatty acid composition of PC of dissected oilseed rape seeds

Supplemental Table S9. Fatty acid composition of phosphatidylinositol of dissected oilseed rape seeds

Received November 4, 2016; accepted February 7, 2017; published February 10, 2017.

LITERATURE CITED

Barthole G, To A, Marchive C, Brunaud V, Soubigou-Taconnat L, Berger N, Dubreucq B, Lepiniec L, Baud S (2014) MYB118 represses endosperm maturation in seeds of *Arabidopsis*. Plant Cell **26:** 3519–3537

Bates PD (2016) Understanding the control of acyl flux through the lipid metabolic network of plant oil biosynthesis. Biochim Biophys Acta **1861:** 1214–1225

Bates PD, Browse J (2011) The pathway of triacylglycerol synthesis through phosphatidylcholine in Arabidopsis produces a bottleneck for the accumulation of unusual fatty acids in transgenic seeds. Plant J **68:** 387–399

Bates PD, Fatihi A, Snapp AR, Carlsson AS, Browse J, Lu C (2012) Acyl editing and headgroup exchange are the major mechanisms that direct polyunsaturated fatty acid flux into triacylglycerols. Plant Physiol **160:** 1530–1539

Benning C, Huang ZH, Gage DA (1995) Accumulation of a novel glycolipid and a betaine lipid in cells of *Rhodobacter sphaeroides* grown under phosphate limitation. Arch Biochem Biophys **317:** 103–111

Borisjuk L, Neuberger T, Schwender J, Heinzel N, Sunderhaus S, Fuchs J, Hay JO, Tschiersch H, Braun HP, Denolf P, et al (2013) Seed architecture shapes embryo metabolism in oilseed rape. Plant Cell **25:** 1625–1640

Boughton BA, Thinagaran D, Sarabia D, Bacic A, Roessner U (2016) Mass spectrometry imaging for plant biology: a review. Phytochem Rev **15:** 445–488

Bryant FM, Munoz-Azcarate O, Kelly AA, Beaudoin F, Kurup S, Eastmond PJ (2016) ACYL-ACYL CARRIER PROTEIN DESATURASE2 and 3 are responsible for making omega-7 fatty acids in the Arabidopsis aleurone. Plant Physiol **172:** 154–162

Cahoon EB, Shanklin J (2000) Substrate-dependent mutant complementation to select fatty acid desaturase variants for metabolic engineering of plant seed oils. Proc Natl Acad Sci USA **97:** 12350–12355

Caprioli RM, Farmer TB, Gile J (1997) Molecular imaging of biological samples: localization of peptides and proteins using MALDI-TOF MS. Anal Chem **69:** 4751–4760

Chapman KD, Ohlrogge JB (2012) Compartmentation of triacylglycerol accumulation in plants. J Biol Chem **287:** 2288–2294

Cornett DS, Reyzer ML, Chaurand P, Caprioli RM (2007) MALDI imaging mass spectrometry: molecular snapshots of biochemical systems. Nat Methods **4:** 828–833

Curb JD, Wergowske G, Dobbs JC, Abbott RD, Huang B (2000) Serum lipid effects of a high-monounsaturated fat diet based on macadamia nuts. Arch Intern Med **160:** 1154–1158

Devaiah SP, Roth MR, Baughman E, Li M, Tamura P, Jeannotte R, Welti R, Wang X (2006) Quantitative profiling of polar glycerolipid species from organs of wild-type Arabidopsis and a phospholipase Dα1 knockout mutant. Phytochemistry **67:** 1907–1924

Durrett TP, Benning C, Ohlrogge J (2008) Plant triacylglycerols as feedstocks for the production of biofuels. Plant J **54:** 593–607

Feenstra AD, Hansen RL, Lee YJ (2015) Multi-matrix, dual polarity, tandem mass spectrometry imaging strategy applied to a germinated maize seed: toward mass spectrometry imaging of an untargeted metabolome. Analyst (Lond) **140:** 7293–7304

Fuschino JR, Guschina IA, Dobson G, Yan ND, Harwood JL, Arts MT (2011) Rising water temperatures alter lipid dynamics and reduce n-3 essential fatty acid concentrations in *Scenedesmus obliquus* (Chlorophyta). J Phycol **47:** 763–774

Gunstone F, Harwood J, Dijkstra A, editors (2007) The Lipid Handbook, Ed 3. CRC Press, Boca Raton, FL

Hankin JA, Barkley RM, Murphy RC (2007) Sublimation as a method of matrix application for mass spectrometric imaging. J Am Soc Mass Spectrom **18:** 1646–1652

Harwood JL, Guschina IA (2013) Regulation of lipid synthesis in oil crops. FEBS Lett **587:** 2079–2081

Haslam RP, Sayanova O, Kim HJ, Cahoon EB, Napier JA (2016) Synthetic redesign of plant lipid metabolism. Plant J **87:** 76–86

Horn PJ, Chapman KD (2013) Metabolite Imager: customized spatial analysis of metabolite distributions in mass spectrometry imaging. Metabolomics **10:** 337–348

Horn PJ, Chapman KD (2014) Lipidomics in situ: insights into plant lipid metabolism from high resolution spatial maps of metabolites. Prog Lipid Res **54:** 32–52

Horn PJ, Korte AR, Neogi PB, Love E, Fuchs J, Strupat K, Borisjuk L, Shulaev V, Lee YJ, Chapman KD (2012) Spatial mapping of lipids at cellular resolution in embryos of cotton. Plant Cell **24:** 622–636

Horn PJ, Silva JE, Anderson D, Fuchs J, Borisjuk L, Nazarenus TJ, Shulaev V, Cahoon EB, Chapman KD (2013) Imaging heterogeneity of membrane and storage lipids in transgenic *Camelina sativa* seeds with altered fatty acid profiles. Plant J **76:** 138–150

Korte AR, Yandeau-Nelson MD, Nikolau BJ, Lee YJ (2015) Subcellular-level resolution MALDI-MS imaging of maize leaf metabolites by MALDI-linear ion trap-Orbitrap mass spectrometer. Anal Bioanal Chem **407:** 2301–2309

Lee J, Welti R, Schapaugh WT, Trick HN (2011) Phospholipid and triacylglycerol profiles modified by PLD suppression in soybean seed. Plant Biotechnol J **9:** 359–372

Li Y, Beisson F, Pollard M, Ohlrogge J (2006) Oil content of Arabidopsis seeds: the influence of seed anatomy, light and plant-to-plant variation. Phytochemistry **67:** 904–915

Li-Beisson Y, Shorrosh B, Beisson F, Andersson MX, Arondel V, Bates PD, Baud S, Bird D, DeBono A, Durrett TP, et al (2010) Acyl-lipid metabolism. The Arabidopsis Book **8:** e0133,

Liu J, Hua W, Yang H, Guo T, Sun X, Wang X, Liu G, Wang H (2014) Effects of specific organs on seed oil accumulation in *Brassica napus* L. Plant Sci **227:** 60–68

Neuberger T, Rolletschek H, Webb A, Borisjuk L (2009) Non-invasive mapping of lipids in plant tissue using magnetic resonance imaging. *In* D Armstrong, ed, Lipidomics. Humana Press, Totawa, NJ, pp 485–496

Neuberger T, Sreenivasulu N, Rokitta M, Rolletschek H, Göbel C, Rutten T, Radchuk V, Feussner I, Wobus U, Jakob P, et al (2008) Quantitative imaging of oil storage in developing crop seeds. Plant Biotechnol J **6:** 31–45

Nguyen HT, Mishra G, Whittle E, Pidkowich MS, Bevan SA, Merlo AO, Walsh TA, Shanklin J (2010) Metabolic engineering of seeds can achieve levels of ω-7 fatty acids comparable with the highest levels found in natural plant sources. Plant Physiol **154:** 1897–1904

Nguyen HT, Park H, Koster KL, Cahoon RE, Nguyen HTM, Shanklin J, Clemente TE, Cahoon EB (2015) Redirection of metabolic flux for high levels of omega-7 monounsaturated fatty acid accumulation in camelina seeds. Plant Biotechnol J **13:** 38–50

Ohlrogge JB, Jaworski JG (1997) Regulation of fatty acid synthesis. Annu Rev Plant Physiol Plant Mol Biol **48:** 109–136

Penfield S, Rylott EL, Gilday AD, Graham S, Larson TR, Graham IA (2004) Reserve mobilization in the *Arabidopsis* endosperm fuels hypocotyl elongation in the dark, is independent of abscisic acid, and requires PHOSPHOENOLPYRUVATE CARBOXYKINASE1. Plant Cell **16:** 2705–2718

Radchuk V, Borisjuk L (2014) Physical, metabolic and developmental functions of the seed coat. Front Plant Sci **5:** 510

Rossak M, Smith M, Kunst L (2001) Expression of the FAE1 gene and FAE1 promoter activity in developing seeds of Arabidopsis thaliana. Plant Mol Biol **46:** 717–725

Schmid M, Davison TS, Henz SR, Pape UJ, Demar M, Vingron M, Schölkopf B, Weigel D, Lohmann JU (2005) A gene expression map of *Arabidopsis thaliana* development. Nat Genet **37:** 501–506

Smith KI, Douce R, Harwood JL (1982) Phospholipid metabolism in the brown alga, *Fucus serratus*. Phytochemistry **21:** 569–573

Sturtevant D, Dueñas ME, Lee YJ, Chapman KD (2017a) Three-dimensional visualization of membrane phospholipid distributions in Arabidopsis thaliana seeds: a spatial perspective of molecular heterogeneity. Biochim Biophys Acta **1862:** 268–281

Sturtevant D, Horn P, Kennedy C, Hinze L, Percy R, Chapman K (2017b) Lipid metabolites in seeds of diverse Gossypium accessions: molecular identification of a high oleic mutant allele. Planta **245:** 595–610

Sturtevant D, Lee YJ, Chapman KD (2016) Matrix assisted laser desorption/ionization-mass spectrometry imaging (MALDI-MSI) for direct visualization of plant metabolites in situ. Curr Opin Biotechnol **37:** 53–60

Wallis JG, Browse J (2002) Mutants of Arabidopsis reveal many roles for membrane lipids. Prog Lipid Res **41:** 254–278

Wang X, Long Y, Yin Y, Zhang C, Gan L, Liu L, Yu L, Meng J, Li M (2015) New insights into the genetic networks affecting seed fatty acid concentrations in *Brassica napus*. BMC Plant Biol **15:** 91

Weselake RJ, Taylor DC, Rahman MH, Shah S, Laroche A, McVetty PBE, Harwood JL (2009) Increasing the flow of carbon into seed oil. Biotechnol Adv **27:** 866–878

Wu Y, Li R, Hildebrand DF (2012) Biosynthesis and metabolic engineering of palmitoleate production, an important contributor to human health and sustainable industry. Prog Lipid Res **51:** 340–349

Zhou Z, Marepally SR, Nune DS, Pallakollu P, Ragan G, Roth MR, Wang L, Lushington GH, Visvanathan M, Welti R (2011) LipidomeDB data calculation environment: online processing of direct-infusion mass spectral data for lipid profiles. Lipids **46:** 879–884